

OBSERVATIONS OF THE INTERSTELLAR MEDIUM IN THE MAGELLANIC BRIDGE<sup>1</sup>N. LEHNER<sup>2,4</sup>, K. R. SEMBACH<sup>3</sup>, P. L. DUFFTON<sup>2</sup>, W. R. J. ROLLESTON<sup>2</sup> AND F. P. KEENAN<sup>2</sup>*Draft version May 20, 2019*

## ABSTRACT

We present ultraviolet and optical spectra of DI 1388, a young star in the Magellanic Bridge, a region of gas between the Small and Large Magellanic Clouds. The data have signal-to-noise ratios of 20–45 and a spectral resolution of  $6.5 \text{ km s}^{-1}$ . Interstellar absorption by the Magellanic Bridge at  $v_{\text{LSR}} \approx 200 \text{ km s}^{-1}$  is visible in the lines of C I, C II, C II\*, C IV, N I, O I, Al II, Si II, Si III, Si IV, S II, Ca II, Fe II, and Ni II. The relative gas-phase abundances of C II, N I, O I, Al II, Si II, Fe II, and Ni II with respect to S II are similar to those found in Galactic halo clouds, despite a significantly lower metallicity in the Magellanic Bridge. The higher ionization species in the cloud have a column density ratio  $N(\text{C}^{+3})/N(\text{Si}^{+3}) \sim 1.9$ , similar to that inferred for collisionally ionized Galactic cloud interfaces at temperatures  $\sim 10^5 \text{ K}$ . We identify sub-structure in the stronger interstellar lines, with a broad component (FWHM  $\sim 20 \text{ km s}^{-1}$ ) at  $\sim 179 \text{ km s}^{-1}$  and a sharp component (FWHM  $\sim 11 \text{ km s}^{-1}$ ) at  $198 \text{ km s}^{-1}$ . The abundance analysis for these clouds indicates that the feature at  $198 \text{ km s}^{-1}$  consists of a low electron density, mainly neutral gas that may be associated with an interface responsible for the highly ionized gas. The  $179 \text{ km s}^{-1}$  cloud consists of warmer, lower density gas that is partially ionized.

*Subject headings:* Galaxies: abundances — ISM: abundances — Magellanic Bridge — ISM: structure

## 1. INTRODUCTION

The Large (LMC) and Small (SMC) Magellanic Clouds are two small irregular galaxies in orbit around the Galaxy, with the LMC being approximately 3 to 10 times more massive than the SMC (Dopita 1990). Distance estimates for the LMC and SMC are  $\sim 49$  and  $\sim 60$  kpc, respectively (see e.g., van den Bergh 1999 and references therein). Evidence for interactions between the Milky Way and the Magellanic Clouds is provided by several high velocity gas complexes connected to the Clouds: the Magellanic Bridge (MB), a  $10^\circ$  region of H I linking the body of the SMC to an extended arm of the LMC; the Magellanic Stream, a  $10^\circ \times 100^\circ$  H I filament that trails the Clouds; and the Leading Arm, a diffuse H I region that leads the Galaxy and the Clouds (Putman 2000). Using data from the H I Parkes All-Sky Survey (HIPASS), Putman (2000) showed that the “boundary” between the SMC and the MB occurs at  $l = 295^\circ$ ,  $b = -41.5^\circ$ , where the H I column density is  $\sim 10^{21} \text{ cm}^{-2}$ . The H I column density slowly decreases toward the LMC to  $\sim 10^{20} \text{ cm}^{-2}$  at the LMC boundary near  $l = 287^\circ$ ,  $b = -35.5^\circ$ . The LSR velocity of the MB gas observed in 21 cm emission ranges from  $\sim 100$  to  $350 \text{ km s}^{-1}$  (McGee and Newton 1986).

Various formation mechanisms for the Bridge, Stream, and Leading Arm have been suggested over the years, and it is now generally agreed that the MB formed via a tidal encounter between the two Clouds. Gardiner and Noguchi (1996) have produced models that can reproduce simultaneously both the MB and the Stream observations. They find that the Bridge was most likely pulled from the wing

of the SMC 200 Myr ago during a close encounter between the two Clouds, whereas the Stream was created by a SMC-LMC-Galaxy close encounter  $\sim 1.5$  Gyr ago.

Searches for stars in the Stream have produced largely negative results (see Irwin et al. 1990 and references therein). However, photographic surveys employing automatic scans of Schmidt plates have now firmly established the existence of blue stellar objects within the MB (Irwin et al. 1990). Subsequent CCD photometry (Demers and Battinelli 1998) and spectroscopy (Rolleston et al. 1999) have shown that the MB contains massive, young ( $< 20$  Myr) stars located between the LMC and SMC. These stars have a metal abundance  $\sim 1.1$  dex lower than their Population I Galactic analogues and  $\sim 0.5$  dex lower than the SMC (Hambly et al. 1994; Rolleston et al. 1999). Their evolutionary lifetimes indicate that star formation is still occurring in the MB, but probably via different mechanisms than those in the Galaxy, as the MB has a very low H I column density (but note the recent detection of cool H I clouds in the MB by Kobulnicky and Dickey (1999), indicating that some regions have relatively high densities).

The combination of high spectral resolution and high sensitivity available with space-based ultraviolet telescopes makes it feasible to investigate the chemical composition and the physical conditions in various interstellar environments in the Galaxy and Magellanic Clouds (see Savage and Sembach 1996 for a review). Here, we report the results of a programme to investigate the chemical composition and abundance pattern of the MB gas with the Hubble Space Telescope (*HST*) and the Space Telescope

<sup>1</sup>Based on observations with the NASA/ESA Hubble Space Telescope, obtained at the Space Telescope Science Institute, which is operated by the Association of Universities for Research in Astronomy, Inc. under NASA contract No. NAS5-26555.

<sup>2</sup>Department of Pure and Applied Physics, The Queen’s University of Belfast, Belfast, BT7 1NN, Northern Ireland

<sup>3</sup>The Johns Hopkins University, Department of Physics and Astronomy, Bloomberg Center, 3400 N. Charles Street, Baltimore, MD 21218, USA

<sup>4</sup>Present address: The Johns Hopkins University, Baltimore, MD 21218, USA

Imaging Spectrograph (STIS). For this investigation, we have chosen a sight line for which Ca II absorption was detected previously by Hambly et al. (1994).

## 2. OBSERVATIONS AND DATA REDUCTIONS

### 2.1. DI 1388

Previously, we obtained high resolution optical spectra for a number of B-type stars in the Magellanic Bridge using the 3.9 m Anglo-Australian Telescope (AAT), during observing runs in 1992 November and 1995 December. One of the stars observed by Hambly et al. (1994), DI 1388, is situated approximately mid-way between the SMC and LMC ( $l = 291.2^\circ$ ,  $b = -41.2^\circ$ ). Interstellar Ca II K absorption at a LSR velocity of  $200 \text{ km s}^{-1}$  has been detected toward DI 1388 (Rolleston et al. 1999). This velocity is consistent with that of the Bridge material seen in H I 21 cm emission (McGee and Newton 1986; Putman 2000). DI 1388 has relatively weak optical stellar absorption lines and a high projected rotational velocity. DI 1388 has the weakest MB ISM Ca II absorption in the Rolleston et al. (1999) sample ( $W_\lambda \sim 42 \text{ m}\AA$ ).

Recent work (Ryans, priv. comm.) classifies DI 1388 as a main-sequence, very early B-type or late O-type star. In Table 1 we summarize its atmospheric and other observational parameters.

### 2.2. HST STIS spectra

HST STIS spectra of DI 1388 were obtained on 1997 November 21. The data are catalogued in the HST archive under the identification O4A801010. A total exposure time of 26,160 seconds was obtained with the far-UV échelle spectrograph (FUV,  $1150\text{--}1730 \text{ \AA}$ ) using the FUV-MAMA detector in the ACCUM mode. The E140M grating was employed centered at  $1425 \text{ \AA}$ , with a  $0.2' \times 0.06'$  slit in order to obtain the highest resolution available with this grating. This configuration resulted in a two-pixel (FWHM) resolution of  $\sim 6.5 \text{ km s}^{-1}$ . Table 2 summarizes the ions observed toward DI 1388 and the respective S/N levels in the nearby stellar continuum.

Data were reduced within the NOAO IRAF package (Morris and Privett 1995) using the STSDAS packages. Standard calibration and extraction procedures were employed using the CALSTIS routine. The spectra from the four different exposures were co-added. Spectral regions containing interstellar lines were normalized by fitting low-order polynomials ( $\leq 4$ , varying with the complexity of the continuum shape) to continuum regions. No special processing to adjust the background levels was necessary (e.g., Howk and Sembach 2000). The cores of the strongly saturated interstellar lines of C II  $\lambda 1334$ , O I  $\lambda 1302$ , and Si II  $\lambda 1304$  are within 1–2% of the zero-flux level, indicating that the uncertainties introduced by scattered light are small for the weaker absorption features analyzed in this study (see Figure 1). At wavelengths shortward of Ly $\alpha$  spurious structures might be present near some lines (e.g., N I, Si II), but the S/N is lower and it is possible that some of these features are simply random noise fluctuations.

### 2.3. AAT observations

Subsequent high resolution optical observations were undertaken on 1999 October with the AAT to obtain both

a high quality spectrum of the interstellar Ca II K line and to detect stellar features. The coudé University College London Echelle Spectrograph (UCLES) was employed with a Tektronix CCD detector, and the dispersing element was a 31.6 lines/mm grating. Bias and quartz lamp flatfield exposures were taken at the start and end of each night. Additionally, ThAr exposures were interleaved with the observations to allow wavelength calibration and to determine the spectral resolution of the data. This instrument configuration resulted in a FWHM velocity resolution of  $\sim 7.1 \text{ km s}^{-1}$  and a signal-to-noise ratio of 45 in the continuum.

The optical data were reduced within the NOAO IRAF package. Standard procedures were followed in all cases, with images being debiased, flatfield corrected, trimmed and cleaned of cosmic rays. The spectra were traced and sky subtracted. Wavelength calibration was performed by identifying the locations of emission lines in the relevant arc spectra. The one dimensional spectra were normalized by fitting a low-order polynomial to continuum regions. Cross-correlation techniques were used to align the individual spectra. The spectra were then weighted by the continuum signal-to-noise levels and co-added.

## 3. ANALYSIS

### 3.1. Spectra and equivalent widths

We transformed the spectra to the dynamical LSR (Mihalas and Binney 1981) using corrections obtained from the STARLINK RV package (Wallace and Clayton 1996). We then modeled the interstellar lines using the optimized Gaussian fitting routines in the STARLINK DIPSO package (Howarth et al. 1996) to obtain radial velocities and equivalent widths. The correction for the HST spectra in the direction of DI 1388 is  $v_{\text{LSR}} - v_{\text{helio}} = 10.7 \text{ km s}^{-1}$ . The MB H I emission has LSR velocities between 100 and  $350 \text{ km s}^{-1}$ . Thus, we assumed that absorption at LSR velocities lower than  $100 \text{ km s}^{-1}$  is from the Milky Way disk and halo, while that at  $v_{\text{LSR}} = 200 \text{ km s}^{-1}$  was assumed to arise in the Magellanic Bridge (see Figure 1). In the HST STIS DI 1388 spectra, a high-velocity cloud (HVC) absorption is present at  $v_{\text{LSR}} = 79.7 \pm 3.4 \text{ km s}^{-1}$  (see Lehner et al. 2000). In Figure 1, we note the detection of very weak features in the spectra of C II  $\lambda 1334$  and Si II  $\lambda\lambda 1193$  and 1260 at LSR velocities of 113 and  $130 \text{ km s}^{-1}$ . The velocities of these two weak HVCs suggest that they are associated with the MB (Lehner et al. 2000).

To check the consistency between absorption line velocities in the optical and ultraviolet absorption spectra, we compared the low velocity portions of the Ni II  $\lambda 1370$  and Ca II K lines. These two lines have roughly the same strength and component structure. The difference in the LSR velocities of the two lines is less than  $3 \text{ km s}^{-1}$ , which is less than the instrumental resolution of either dataset. The absorption profile velocities also agree well with those of H I emission observations obtained with the ATCA (Lehner et al. 1999a) and Parkes (Putman, priv. comm.) telescopes. As a final check, we compared the stellar radial velocities in both the optical and ultraviolet spectra of DI 1388 and found them to be consistent within their uncertainties.

Table 2 presents the equivalent width results for the MB absorption. The S/N ratios are sufficient to detect two

components in many of the stronger lines arising in the MB; this structure manifests itself as the combination of a broad component at  $179 \text{ km s}^{-1}$  and a narrow component at  $198 \text{ km s}^{-1}$  (see Figures 1 and 2 and discussion in Section 3.3). Owing to the large stellar projected rotational velocity, contamination by stellar absorption is generally unimportant for the MB absorption, except for the higher ion lines of C IV, Si III and Si IV, as illustrated in Figure 1.

Errors on the equivalent widths in Table 2 are  $1\sigma$  estimates, including statistical noise fluctuations in the lines and systematic errors arising from continuum placement uncertainties. The latter were obtained by changing the continuum by an amount equal to  $\sim 0.2 - 0.4$  times the RMS noise value, where the scale factor 0.2 corresponds to a flat continuum and 0.4 to a continuum with large curvature (Sembach and Savage 1992). The  $3\sigma$  upper limits for the equivalent widths are defined as  $W_{\min} = 3\sigma 2\delta\lambda$ , where  $\sigma$  is the inverse of continuum S/N ratio,  $\delta\lambda$  is the spectral resolution in mÅ, and  $2\delta\lambda$  reflects approximately the FWHM of the absorption lines (see Table 3). Other errors such as background and scattered light uncertainties are not included but are expected to be small since the zero-level is relatively well determined (see Section 2.2).

### 3.2. Apparent column density profiles

We used the apparent optical depth method to derive column densities and to check for unresolved saturated structures within the observed profiles (Savage and Sembach 1991). We converted the normalized absorption profiles into apparent optical depths per unit velocity,  $\tau_a(v) = \ln[1/I_{\text{obs}}(v)]$ , where  $I_{\text{obs}}$  is the normalized observed intensity. These values of  $\tau_a(v)$  are related to the apparent column densities per unit velocity,  $N_a(v)$  ( $\text{cm}^{-2} (\text{km s}^{-1})^{-1}$ ) through the relation  $N_a(v) = 3.768 \times 10^{14} \tau_a(v) / [f\lambda(\text{\AA})]$ . A direct integration of the apparent column density profiles over the velocity range yields the total column densities of the lines, provided there are no unresolved saturated structures present (Savage and Sembach 1991). We adopted wavelengths and oscillator strengths from the Morton (1991) atomic data compilation unless otherwise indicated in Table 2.

The last column of Table 2 gives the resulting column densities<sup>5</sup> for the different ions in the MB gas observed toward DI1388. Errors on the column densities are  $1\sigma$  estimates (see the equivalent width uncertainties in Section 3.1). Upper limits ( $3\sigma$ ) are obtained from the corresponding equivalent width limit and the assumption of a linear curve of growth. Lower limits indicate that the line contains some unresolved, saturated absorption that cannot be reliably estimated with the existing data. In the absence of unresolved saturated structure, two or more lines of a given species with different values of  $f\lambda$  will have the same distribution of  $N_a(v)$ . Differences in  $N_a(v)$  suggest that some saturation is present for the stronger line(s). Figure 3 clearly demonstrates this for the MB Si II lines; no unresolved saturated absorption is observed for Si II  $\lambda\lambda 1304$  and 1526, while  $\lambda 1190$  is slightly saturated and  $\lambda 1193$  is strongly saturated. The other singly ionized species follow a similar curve of growth (similar  $b$ -values – see Section 3.3), and therefore the weaker singly ion-

ized lines are not saturated. C II  $\lambda 1334$  and Si III  $\lambda 1206$  are stronger lines that may contain some unresolved saturated structures at the MB velocity. The N I lines have lower effective  $b$ -values that place them on the flat part of the curve of growth. This is confirmed in Figure 3, where comparison of the apparent column density profiles for the different lines shows that some unresolved saturated structure is present (as expected for narrower features). O I  $\lambda 1302$ , which probably follows a curve of growth similar to that of the singly ionized species, is strong and probably contains some unresolved saturated structure.

### 3.3. Component-fitting measurements

For the relatively strong lines of C II, N I, O I, Al II, Si II, S II, Fe II, and the Ca II line, we also used a Voigt profile fitting method (Welty et al. 1991) to measure the column densities and the  $b$ -values. We modeled these features first with the optimized Gaussian fitting routines (ELFINP) in the STARLINK package DIPSO (Howarth et al. 1996) to obtain radial velocities, equivalent widths, and the full widths at half maximum intensity (FWHM =  $2\sqrt{\ln 2} b$ , where  $b^2 = 2kT/(Am) + v_{\text{turb}}^2$ , and  $A$  and  $m$  are the ion mass in atomic mass units and the hydrogen mass, respectively). We then used two of the three parameters from the fit ( $v_{\text{LSR}}$ ,  $b$ ) as initial estimates in the Voigt profile fitting programme. The results of this process are summarized in Table 3, and some spectra with their respective fits are presented in Figure 2. The errors in this table are  $1\sigma$  estimates, including statistical noise fluctuations in the lines and systematic errors due to uncertainties in the continuum placement (see previous section). We note that the component fit results are consistent with the apparent optical depth column densities.

The C II, O I, Al II, Si II, S II, and Fe II features have a two-component structure, with a broad feature centered at  $\sim 179 \text{ km s}^{-1}$  and sharp component at  $\sim 198 \text{ km s}^{-1}$ . The fit for the strong C II line is uncertain because of the strength of the line. The fit for the Al II line is also uncertain since the line falls near the edge of an échelle order and is not completely covered in these data. The  $b$ -values for S II appear to be smaller than for the other absorption lines. However, for  $b$ -values between 7 and 10  $\text{km s}^{-1}$  (typical values for the other lines), the derived S II column densities do not change by more than the  $1\sigma$  error indicated in Table 3. The residuals in the fit for O I indicate that the sharp component contains either some unresolved saturated structures or additional weak components. The column density of the broader O I component is also somewhat uncertain as it lies on the flat part of the curve of growth. The N I lines exhibit a well-defined sharp component at  $\sim 198 \text{ km s}^{-1}$ , but the broad component is not detected in the  $\lambda 1200$  line and is very weak in the  $\lambda 1201$  line. The N I  $\lambda 1200$  non-detection could be due to the continuum uncertainties on the blue side of this line (see Figure 1). For the weak C II\* and Ni II lines, the S/N ratios of the data allow identification of only the sharp component. Finer structure seen in higher resolution spectra of Galactic HVCs (Ryans et al. 1996; Lehner et al. 1999b) suggests that the true component structure in the MB gas toward DI 1388 may be more complex than

<sup>5</sup>In this table N I  $\lambda 1199$  and Fe II  $\lambda 1260$  column densities were obtained by component fitting to deblend the lines from lower velocity components and other species.

is revealed by our data.

#### 4. OVERVIEW OF SPECIES OBSERVED IN THE MAGELLANIC BRIDGE

The wide range of ionization states observed for the MB shows that the ionization structure of these clouds is complex, as the clouds exhibit species ranging from neutral gas tracers (e.g., O I and N I) to triply ionized gas tracers (e.g., Si IV and C IV). Before interpreting the derived column densities, we present a short description of the observed species and the roles that they might play within the neutral and ionized environments.

**- C I, C II, C II\*, C IV:** The MB component contains a strong, saturated C II  $\lambda\lambda 1334$  absorption feature and a moderately strong C II\*  $\lambda 1335$  line. Individual C I lines are not detected at significant levels. We weighted the C I lines by their  $gf$  values and S/N levels and co-added the lines to produce an average C I line. This resulted in a tentative detection at  $198.1 \text{ km s}^{-1}$  (Figure 4); the derived column density is  $\approx 12.26 \text{ dex}$ . The interstellar C IV lines are blended with a broad, deep stellar line centered at  $\sim 150 \text{ km s}^{-1}$ . We approximated the stellar C IV absorption with a Gaussian profile to produce the interstellar column density listed in Table 2. The effect of this deblending is shown in Figure 2. C II is the dominant ionization stage in both the warm neutral medium (WNM) and warm ionized medium (WIM) (Sembach 1995; Sembach et al. 2000), while C IV is primarily produced by collisional ionization at  $T_e \sim 10^5 \text{ K}$  (Sutherland and Dopita 1993). The combination of C I, C II and C IV absorption in the Bridge suggests that there may be interfaces between hot and cool regions.

**- N I and O I:** N I and O I are excellent tracers of neutral gas as their ionization potentials and charge exchange reactions with hydrogen ensure that they are primarily found in H I regions. Magellanic Bridge N I is observed at 1199, 1200 and 1201 Å, but the 1199 Å line is blended with the saturated local absorption in the N I  $\lambda 1200$  line. The mean column density of N I in the MB is greater than  $14.0 \text{ dex}$ . O I  $\lambda 1302$  is also detected in the MB and is very strong.

**- Si II, Si III and Si IV:** These ions are observed at the velocities of the MB. Si II is the dominant ion in both the WNM and WIM (Sembach et al. 2000). For Si II  $\lambda\lambda 1304$  and 1526, we have adopted the oscillator strengths of Dufton et al. (1983, 1992), as recent studies indicate that they are more accurate than other estimates (Spitzer and Fitzpatrick 1993), and indeed the derived column densities for the different Si II lines agree well. Strong Si III  $\lambda 1206$  absorption present at MB velocities is partially blended with a broad stellar feature. Removing the deepest possible stellar line centered at  $150 \text{ km s}^{-1}$ , we find a column density of  $> 13.45 \text{ dex}$  for the MB Si III absorption (see Table 2). The Si III line shape differs substantially from that of the singly ionized species in that the the  $198 \text{ km s}^{-1}$  component is much broader ( $b \sim 16 \text{ km s}^{-1}$ ). The presence of Si III suggests that the gas could be partially ionized. Si IV is also present in the MB, indicating that some hotter ( $T \sim 10^5 \text{ K}$ ) gas may also exist. We estimated the Si IV line strengths by deblending the stellar absorption using the same strategy employed for C IV. The detection of Si III, Si IV, and C IV at velocities similar to the neutral and low-ionization species indicates that

the hot component is not circumstellar.

**- S II and S III:** Sulfur is found mainly in the gas phase (Savage and Sembach 1996) and can be used as a reference to study the depletions of other elements in the gas. The S II  $\lambda\lambda 1250$  and 1253 lines are weak but definitely detected, while the feature at 1259 Å is blended with the strong saturated local Si II  $\lambda 1260$  absorption. S III is not detected.

**- Al II, Ca II, Fe II, Ni II:** These species are grouped together as they have the general property of being readily depleted on to dust grains (Savage and Sembach 1996). With the exception of Ca II, these species are dominant in the neutral and ionized gas (though Fe III can be dominant in some ionized gas – see e.g. Sembach et al. 2000). Only part of the Al II  $\lambda 1670$  MB feature is present in the *HST* STIS spectrum, so it is difficult to measure the line strength accurately. Fe II  $\lambda\lambda 1260$  and 1608 are detected, while  $\lambda 1611$  is not detected. For Fe II  $\lambda\lambda 1608$  and 1611, we have adopted the oscillator strengths of Mullman et al. (1997) and Cardelli and Savage (1995), respectively. Only the measured column density of  $\lambda 1608$  is reliable, as Fe II  $\lambda 1260$  is strongly blended with the saturated MB component of Si II  $\lambda 1260$ . The Ni II absorption lines are very weak. For Ni II, recent studies (Fedchak and Lawler 1999; Zsargó and Federman 1998) suggest that the oscillator strengths are lower by a factor 0.53 compared to the previous values; we have therefore adopted this scaling factor. To improve the reliability of Ni II column density, the three spectra were co-added using a method similar to that employed for C I. The result is shown in Figure 4, where the centroid of the line ( $198.4 \text{ km s}^{-1}$ ) is in good agreement with the centroids of the stronger lines. The  $b$ -value is about  $5.7 \text{ km s}^{-1}$ , a bit smaller than for the other singly ionized lines. The derived Ni II column density is  $12.52 \pm 0.20 \text{ dex}$ .

#### 5. PHYSICAL CONDITIONS WITHIN THE MAGELLANIC BRIDGE GAS

##### 5.1. Depletions

To determine the depletion pattern of the MB, we compared relative heavy element column densities. Since S II is only modestly depleted in the Galactic ISM, we used it as the reference ion. The logarithmic normalized gas-phase abundance is defined using the following notation:

$$[X/S] = \log \left( \frac{X^i}{S^+} \right) - \log \left( \frac{X}{S} \right)_c, \quad (1)$$

where  $X^i$  is the ion under consideration, and  $(X/S)_c$  is the ratio for cosmic abundances and  $X/S$  is used for  $N(X)/N(S)$ . Equation 1 assumes that the ion  $X^i$  is the dominant form of element  $X$ . When it is not, we will consider explanations other than depletion on to dust grains (such as ionization) for the derived deficiencies. The normalized gas-phase abundances observed in the MB, derived from Equation 1, are given in Table 4 and plotted in Figure 5 for the total column density derived from the apparent optical depth method. Table 5 and Figure 6 show the relative abundance patterns for the two components at  $179$  and  $198 \text{ km s}^{-1}$ .

Previous ISM studies using high spectral resolution and high S/N ratio UV data have shown a general progression of increasingly severe depletion from warm halo clouds, to

warm disk clouds, to colder disk clouds. Therefore, we compare the depletion in the MB to the depletion patterns observed in those three representative Galactic environments. The Galactic results from previous UV studies (Jenkins 1987; Savage and Sembach 1996; Fitzpatrick 1996; Welty et al. 1999b) are summarized in Table 4. Note that the halo values for C, N, O, and Al from Welty et al. (1999b) are estimated values since no actual measurements yet exist. Figure 5 shows the comparison between the different Galactic environments and the results for the MB. However, in order to compare the depletion pattern of the MB with those in the Galaxy, it may be necessary to correct the former for any differences in the underlying (undepleted) total elemental abundance for the MB and Galaxy. For the LMC and SMC abundances we have adopted the results of Russell and Dopita (1992, and references therein, but see also Garnett 1999, Korn and Wolf 1999), except for Al (see discussion in Welty et al. 1997, 1999 and references therein), and LMC Si abundance which is from Korn and Wolf (1999). The last two columns in Table 4 summarize these abundances, where the errors on  $[X/S]_{\text{SMC/LMC}}$  are typically  $\pm 0.2$  dex.

In Figures 5 and 6, we indicate the corrections of the MB depletions assuming  $(X/S)_{\text{MB}} = (X/S)_{\text{SMC}}$ , as most of the MB gas may arise from the SMC (Gardiner and Noguchi 1996, Rolleston et al. 1999 – but see discussion in Section 6). The MB depletions of Si, Fe, and Ni in the MB are very similar to the Galactic halo pattern, both with or without these corrections (see Figure 5). The component analysis in Figure 6 leads to the same conclusion for Si and Fe for the individual components. The lower limits of C II, N I, and O I also are consistent with the Galactic depletion pattern. However, when the cloudlet sub-structure is considered the non-saturated broader component of N I appears to be underabundant by  $-1.3$  dex (or  $-0.7$  dex when the SMC corrections are applied). The Al II lower limit is consistent with the (estimated) Galactic halo depletion value.

### 5.2. Temperature and density of the gas

In principle, the component  $b$ -values can be used to determine the kinetic temperature of the gas. For the sharper component of N I, O I, Si II and Fe II, the inferred temperature has an uncertainty as large as the value itself. However, for the narrower component of N I, we can place an upper limit on the temperature,  $T < 1.7 \times 10^4$  K. The detections of O I and N I suggest  $T < 10^4$  K, since at higher temperatures most of the O and N would be ionized due to collisions (Sembach 1995).

If collisions with electrons are the principal source of excitation of C II\* in the MB, then the familiar equation between C II and C II\* (Spitzer and Fitzpatrick 1993) can be written as

$$n_e = \frac{1}{5.46} T^{0.5} \frac{n(\text{C}^{++})}{n(\text{C}^+)} \text{ cm}^{-3}. \quad (2)$$

This relation provides an estimate of the electron density when the space densities are replaced by column densities, and therefore we make the standard supposition that the two excited states are spatially coincident along the sight line. C II is strongly saturated, so we use S II as a proxy for C II after scaling by the appropriate relative cosmic abundance and relative depletion of  $-0.3$  dex (Spitzer and

Fitzpatrick 1993), so that  $N(\text{C}^+) \sim 5 - 10 \times N(\text{S}^+)$  (the factor 10 is appropriate for the Galaxy – e.g. Spitzer and Fitzpatrick 1993, while the factor of 5 accounts for the metallicity of the SMC – Russell and Dopita 1992). These ions are also the dominant ionization stages in both the neutral and ionized gas, and assuming that they are spatially coincident along the sight line, the electron density is:  $n_e \sim 5 - 10 \times 10^{-4} T^{0.5} \text{ cm}^{-3}$ . For  $T < 1.7 \times 10^4$  K,  $n_e < 0.05 - 0.10 \text{ cm}^{-3}$ . This density is derived from the total column densities of the ions, which are dominated by the strong, sharp component at  $198 \text{ km s}^{-1}$ . The cloud at  $179 \text{ km s}^{-1}$  is expected to be a low density gas as it is partially ionized (See Section 6.1).

If ionization equilibrium applies ( $\Gamma N(\text{X}^0) = \alpha n_e N(\text{X}^+)$ ), the ratio of photoionization rates to recombination rates,  $\Gamma/\alpha$ , can be estimated using the tentative measurement of C I, the estimate of C II and the upper limit on  $n_e$ :  $\Gamma/\alpha < 24 - 48$ . For comparison, in the Galaxy  $\Gamma/\alpha \approx 25$  ( $T = 100$  K),  $\Gamma/\alpha \approx 48$  ( $T = 300$  K),  $\Gamma/\alpha \approx 100$  ( $T = 1000$  K) (Péquignot and Aldrovandi 1986, for the WJ1 radiation field) which indicates that either the MB radiation field is lower than the typical Galactic field or that the temperature of the gas is low.

### 5.3. Highly ionized species

The detection of Si IV and C IV lines in the MB places constraints on the temperature of the highly ionized species. In the Galactic halo, the high ionization absorption average ratios are:  $N(\text{C}^{+3})/N(\text{Si}^{+3}) = 4.6 \pm 2.4$  and  $N(\text{Si}^{+3})/N(\text{N}^{+4}) = 1.2 \pm 0.6$  (Savage et al. 1997). There is also hot gas in the SMC and LMC detected via Si IV and C IV absorption lines (Fitzpatrick and Savage 1985; de Boer and Savage 1980). The recent study of LMC coronal gas by Wakker et al. (1998) seems to suggest that the processes for producing C IV may be similar in both galaxies.

The widths of the MB Si IV and C IV lines imply a temperature of  $< 1.7 \times 10^5$  K. As discussed previously, the process of deblending the Si IV and C IV lines introduces some relatively large uncertainties in their derived column densities. Therefore, instead of considering the total column density results, we plot the ratio  $N_a(\text{C}^{+3})/N_a(\text{Si}^{+3})$  versus the LSR velocity in Figure 7. The observed scatter and differences between the two Si IV  $\lambda\lambda 1393, 1402$  lines in this figure reflect primarily the uncertainties introduced by deblending for the stellar lines. However, we find the average ratio  $N_a(\text{C}^{+3})/N_a(\text{Si}^{+3}) \sim 1.9 \pm 0.9$  to be consistent with values observed along Galactic and extragalactic sight lines. N V is not detected in the DI 1388 spectra (only the stellar lines are detected at 1238.82 and 1242.80 Å), but the measured  $3\sigma$  upper limit of  $\log N(\text{N}^{+4}) < 12.8$  dex (assuming a similar width to Si IV and C IV and that the lines are on the linear part of the curve of growth) implies  $N(\text{Si}^{+3})/N(\text{N}^{+4}) > 1.2$ . This value is compatible with values observed in the lower part of the Galactic halo and indicates that the production of the highly ionized species (Sembach and Savage 1992; Sembach et al. 1997; Savage et al. 1997) may be similar in both the Galactic halo and the MB.

## 6. DISCUSSION

### 6.1. Interpretation of the depletion patterns

In the Galactic ISM, the underabundances of elements along various sight line are usually attributed to the depletion of these elements into dust. The nucleosynthetic history of the gas can also play a role, especially in a low metallicity medium such as the MB. Russell and Dopita (1992; see also Welty et al. 1997, 1999 and references therein) showed that the relative abundances of the  $\alpha$ -elements (Ne, Mg, Si, S, Ar, Ca) and Fe-peak elements (Cr, Fe, Ni, Zn) for the SMC and LMC H II regions and young stars are similar to those found in analogous Galactic objects. Welty et al. (1997, 1999a) presented detailed studies of two Magellanic Clouds sightlines (Sk 108 in the SMC, SN 1987A in the LMC), for which the gas-phase abundance patterns resemble those found either for warm Galactic disk clouds or for clouds in the Galactic halo. They concluded that the similar gas-phase abundance patterns in the three galaxies imply similar depletion patterns, despite global differences in their metal and dust content.

A detailed comparison of the relative stellar abundances in the MB with those in these three galaxies is not yet possible, as the derived absolute stellar abundances are poorly determined and are available only for C, N, O, Mg, and Si (Rolleston et al. 1999). However, differential abundance analyses of the young B-type stars in the MB show that, for those elements, the MB is deficient by  $-1.1 \pm 0.2$  dex relative to the Galaxy. The scatter around this value is fairly small. This result has been confirmed recently in a study of a supergiant star (Rolleston, priv. comm.) and in particular shows that the nitrogen abundance exhibits a similar deficiency (see Section 6.3). Our results show that the abundance pattern in the MB gas toward DI 1388 resembles that found in Galactic halo clouds and in the SMC gas toward Sk 108. Therefore, it seems that the dominant factor describing the MB gas-phase abundance pattern is depletion of the elements into dust rather than nucleosynthetic history. Clearly, additional studies of other MB sight lines would help to test this hypothesis.

The properties of the two MB ISM clouds toward DI 1388 can therefore be summarized as follows:

- The  $198 \text{ km s}^{-1}$  cloud: The gas-phase abundance pattern shown in Figure 6 follows the Galactic halo pattern. The presence of strong O I and N I suggests that much of the gas is neutral. There is no detectable S III, but Si III is detected, suggesting that some ionized gas is also present. This ionized gas may be associated with the more highly ionized gas associated with Si IV and C IV. This cloud consists of a low electron density, mainly neutral gas that might have a hotter, ionized boundary.

- The  $179 \text{ km s}^{-1}$  cloud: The gas-phase abundances of Si II and Fe II shown in Figure 6 indicate that this cloud also follows a Galactic halo depletion pattern. However, N I is remarkably deficient with respect to S II, which probably indicates that the gas is partially ionized. This would also be consistent with the smaller deficiency of Si II and Fe II compared to N I. Similarly, O I is only mildly saturated, which again may indicate that the gas is partially ionized. Si III is present and saturated; but again indicating that a certain amount of gas is partially ionized. S III is not detected, but this is not surprising, as this feature is expected to be weak and below the detection limit of our spectra.

## 6.2. Absolute metallicity of the Bridge gas

Using the HIPASS 21 cm data with a spectral resolution of  $1 \text{ km s}^{-1}$  and a spatial resolution of  $15.5'$ , Putman (priv. comm.) found an H I emission column density  $\log N(\text{H}^0) \simeq 20.30$  dex in the direction of DI 1388. For comparison, the hydrogen column density obtained using S II and scaling by the cosmic reference  $[\text{S}/\text{H}] = -4.73$  dex is  $\log N(\text{H}) \simeq 20.07$  dex after accounting for the metallicity of  $-1.1$  dex. This is in rough agreement with the column density derived from the 21 cm data. Differences could be due to the large beam of the H I emission data and to the position (in depth along the sight line) of DI 1388 in the MB. However, our data generally support a metallicity of  $\sim -1.1$  dex compared to the Galaxy metallicity, confirming the results from the B-type stars study by Rolleston et al. (1999). This implies that the metallicity in the MB does not reflect the SMC metallicity, which is at odds with the tidal model origin of the MB (Gardiner and Noguchi 1996). Rolleston et al. (1999) proposed that the MB gas was formed from a mixture of SMC gas and an unenriched component.

## 6.3. The nitrogen “problem”

The absolute nitrogen abundance in the SMC is still very uncertain as H II regions and stellar analyses yield substantially different results (about 0.5 dex, e.g. Garnett 1999, but see Dufton et al. 1990 for a counter-example). The reasons for this behaviour are still not well understood, mainly because the production mechanisms for N are still poorly constrained (see e.g., discussion in Russell and Dopita 1992, and references therein). However, in principle it should be possible to supplement these analyses with interstellar data for the SMC and the MB since nitrogen is not readily incorporated into dust grains (Meyer et al. 1997).

Our data tentatively suggest that nitrogen is deficient in the MB gas relative to other elements. For the component at  $179 \text{ km s}^{-1}$ ,  $[\text{N}^0/\text{S}^+] = -1.32$  dex. This deficiency is unlikely to be due to depletion of N into grains. N I compared to O I is also largely deficient ( $< -0.5$  dex), which could be due in part to N I being preferentially ionized relative to O and H due its larger photoionization cross section. However, Sofia and Jenkins (1998) indicate that N I is generally a good substitute for H I due to the very fast charge transfer of N II with H I which effectively keeps the ionization fractions of N and H essentially coupled. For the component at  $198 \text{ km s}^{-1}$ , the saturated oxygen and nitrogen lines do not clarify the situation. The amount of N that has been ionized could be checked with *Far Ultraviolet Spectroscopic Explorer* measurements of N II and N III absorptions. A far-UV study would also help to constrain the neutral nitrogen abundance, as there are numerous N I lines in the *FUSE* bandpass that are weaker than the strong 1200 Å lines observed in our STIS spectrum of DI 1388.

## 7. SUMMARY AND CONCLUDING REMARKS

We have presented *HST* STIS E140M UV and AAT optical spectra of the young star DI 1388 located in the Magellanic Bridge. The échelle spectra show interstellar absorption from C I, C II, C II\*, C IV, N I, O I, Al II, Si II, Si III, Si IV, S II, Ca II, Fe II, and Ni II. The relative

gas-phase abundance of the MB ISM gas toward DI 1388 resembles that of gas in the Galactic halo. Since there is independent information on the total abundances from stars and/or nebulae of the Galaxy, SMC, LMC, and MB, the observed abundance pattern in the MB ISM is attributed to varying degrees of depletion onto dust similar to that in halo clouds and SMC toward Sk 108.

Fits to the absorption profiles reveal two MB interstellar components at 179 and 198 km s<sup>-1</sup>. These two clouds along the line of sight have different properties: (1) The cloud at 198 km s<sup>-1</sup> has a temperature  $T < 10^4$  K, low electron density ( $n_e < 0.05\text{--}0.1$  cm<sup>-3</sup>), and is mainly neutral with a possible collisionally ionized boundary detected in Si III, Si IV, and C IV. (2) The cloud at 179 km s<sup>-1</sup> is low density gas, warmer, and partially ionized.

Higher resolution data might allow a more detailed picture of the interstellar structure, which bears on the possibility that these clouds trigger star formation via cloud-cloud collisions (Dyson and Hartquist 1983). As discussed above, star formation is continuing in the MB, as there are young hot stars with evolutionary lifetimes ( $\lesssim 20$  Myr) much younger than the age of the MB ( $\sim 200$  Myr). In all known environments, star formation occurs within molecular clouds or cloud complexes, but there is presently no direct evidence of star-forming gas clouds in the MB. Kobulnicky and Dickey (1999) have detected cold H I clouds in the MB, which suggests the presence of atomic or molecular condensations that could harbor star formation. However, no CO emission has been yet detected (Smoker et al. 2000), and therefore cloud-cloud collisions could be the

dominant star formation trigger.

Finally, we note that this work is relevant to the study of QSO absorption-line systems (QSOALS). Welty et al. (1997, 1999a) propose that the known depletions patterns in the SMC, LMC, and Galaxy may be used to deduce the total elemental abundances in the QSOALS from the observed gas-phase abundances. Indeed, the MB interstellar gas is characterized by modest depletion and metallicity. Moreover, the results of this study and those of Welty et al. (1997, 1999a) suggest that the observed depletion patterns are independent of the metallicity. These patterns could therefore be applied to the QSOALS. Detailed studies of the interstellar medium along other sight lines in the MB, SMC, and LMC should help to know whether these results can be generalized to a wider range of environments.

We are grateful to Mary Putman for providing the HIPASS data toward the general direction of DI 1388 and for useful discussions. We appreciate insightful comments from Chris Howk. NL held a postgraduate studentship from the European Social Fund and Northern Ireland Development for Research through most time of this work. WRJR acknowledges financial support from the UK Particle and Astronomy Research Council. This research has made use of the NASA Astrophysics Data System Abstract Service (<http://adswww.harvard.edu/>) and the CDS database (<http://cdsweb.u-strasbg.fr/>). We thank Dan Welty for his careful reading of the manuscript and insightful comments.

## REFERENCES

Anders, E., Grevesse, N., 1989, *Geochim. Cosmochim. Acta*, 53, 197  
 Cardelli, J. A., Savage, B. D. 1995, *ApJ*, 452, 275  
 de Boer, K. S., Savage, B. D. 1980, *ApJ*, 238, 86  
 Demers, S., Battinelli, P. 1998, *ApJ*, 115, 154  
 Dopita, M. A. 1990, in *The interstellar medium in galaxies*, Proc. of the 2nd Teton conference, Kluwer, Dordrecht  
 Dufton, P. L., Fitzsimmons, A., Howarth, I. D., 1990, *ApJ*, 362, 59  
 Dufton, P. L., Hibbert, A., Kingston, A. E., Tully, J. A. 1983, *MNRAS*, 202, 145  
 Dufton, P. L., Keenan, F. P., Hibbert, A., Ojha, P. C., Stafford, R. P. 1992, *ApJ*, 387, 414  
 Dyson, J. E., Hartquist, T. W. 1983, *MNRAS*, 203, 1233  
 Fedchak, J. A., Lawler, J. E. 1999, *ApJ*, 523, 734  
 Field G. B., Steigman G., 1971, *ApJ*, 166, 59  
 Fitzpatrick, E. L. 1996, *ApJ*, 473, L55  
 Fitzpatrick, E. L., Savage, B. D. 1985, *ApJ*, 292, 122  
 Gardiner, L. T., Noguchi, M. 1996, *MNRAS*, 278, 191  
 Garnett, D. R. 1999, in IAU no. 190 New views of the Magellanic Clouds, ed. Y.-H. Chu et al., p.266  
 Grevesse, N., Noels, A. 1993, in *Origin of the elements*, ed. N. Prantzos et al. (Cambridge: Cambridge Univ. Press), 15  
 Hambly, N. C., Dufton, P. L., Keenan, F. P., Rolleston, W. R. J., Howarth, I. D., Irwin, M. J. 1994, *A&A*, 285, 716  
 Howarth, I. D., Murray, J., Mills, D., Berry, D. S. 1996, *STARLINK User Note SUN 50*, Rutherford Appleton Laboratory/CCLRC  
 Howk, J. C., Sembach, K. R. 2000, *AJ*, 119, 2481  
 Irwin, M. J., Demers, S., Kunkel, W. E. 1990, *AJ*, 99, 191  
 Jenkins, E. B. 1987, in *Interstellar processes*, edd. D.J. Hollenbach & H.A. Thronson (Dordrecht: Reidel), 533  
 Kobulnicky, H. A., Dickey, J. M. 1999, *AJ*, 117, 908  
 Korn, A. J., Wolf, B. 1999, in IAU no. 190 New views of the Magellanic Clouds, ed. Y.-H. Chu et al., p.241  
 Lauroesch, J. T., Truran, J. W., Welty, D. E., York, D. G. 1996, *PASP*, 108, 641  
 Lehner, N., Keenan, F. P., Sembach K. R. 2000, *MNRAS*, in press  
 Lehner, N., et al. 1999a, in IAU no. 190 New views of the Magellanic Clouds, ed. Y.-H. Chu et al., p.501  
 Lehner, N., Sembach, K. R., Lambert, D. L., Ryans, R. S. I., Keenan, F. P. 1999b, *A&A*, 352, 257  
 McGee R. X., Newton L. M., 1986, *PASA*, 6, 471  
 Meyer, D. M., Cardelli, J. A., Sofia, U. J., *ApJ*, L490, 103  
 Mihalas, D., Binney, L. 1981, *Galactic astronomy*, 2nd edition, San Francisco: Freeman  
 Morris, R., Privett, G. 1995, *STARLINK User Note SUN 79*, Rutherford Appleton Laboratory/CCLRC  
 Morton, D. C. 1991, *ApJS*, 77, 119  
 Mullman, K. L., Sakai, M., Lawler, J. E. 1997, *A&AS*, 122, 157  
 Péquignot, D., Aldrovandi, S. M. V. 1986, *A&A*, 161, 169  
 Putman, M. E. 2000, *PASA*, 17, 1  
 Rolleston, W. R. J., Dufton, P. L., McErlean, N. D., Venn, K. A. 1999, *A&A*, 348, 728  
 Russell, S. C., Dopita, M. A. 1992, *ApJ*, 384, 508  
 Ryans, R. S. I., Keenan, F. P., Sembach, K. R. 1996, *A&A*, 289, 539  
 Savage, B. D., Sembach, K. R. 1991, *ApJ*, 379, 245  
 Savage, B. D., Sembach, K. R. 1996, *ARA&A*, 34, 279  
 Savage, B. D., Sembach, K. R., Lu, L. 1997, *AJ*, 113, 2158  
 Sembach, K. R. 1995, *ApJ*, 379, 245  
 Sembach, K. R., Savage, B. D. 1992, *ApJ*, 379, 245  
 Sembach, K. R., Howk, J. C., Ryans, R. S. I., Keenan, F. P. 2000, *ApJ*, 528, 310  
 Sembach, K. R., Savage, B. D., Tripp, T. M. 1997, *ApJ*, 480, 216  
 Smoker, J. V., Keenan, F. P., Polatidis, A., Mooney, C. J., Lehner, N., Rolleston, W. R. J. 2000, *A&A*, in press  
 Sofia, U. J., Fabian, D., Howk, J. C. 2000, *ApJ*, 430, 650  
 Sofia, U. J., Jenkins, E. B. 1998, *ApJ*, 499, 951  
 Spitzer, L., Fitzpatrick, E. L. 1993, *ApJ*, 531, 384  
 Sutherland, R. S., Dopita, M. A. 1993, *ApJS*, 88, 253  
 van den Bergh, S. 1999, in IAU no. 190 New Views of the Magellanic Clouds, ed. Y.-H. Chu et al., p.569  
 Wakker, B. , Howk, J. C., Chu, Y.-H., Bomans, D., Points, S. D., 1998 *ApJ*, 499, L87  
 Wallace, P. T., Clayton, C., 1996 *rv*, *STARLINK User Note SUN 78*, Rutherford Appleton Laboratory/CCLRC  
 Wayte, D. E. 1990, *ApJ*, 355, 473  
 Welty, D. E., Hobbs, L. M., York, D. G. 1991, *ApJS*, 75, 425  
 Welty, D. E., Lauroesch, J. T., Blades, J. C., Hobbs, L. M., York, D. G. 1997, *ApJ*, 489, 672  
 Welty, D. E., Frisch, P. C., Sonneborn, G., York, D. G. 1999a, *ApJ*, 512, 636

Welty, D. E., Hobbs, L. M., Lauroesch, J. T., Morton, D. C., Spitzer, L., York, D. G. 1999b, *ApJS*, 124, 465

Wiese, W. L., Fuhr, J. R., Deters, T. M. 1996, *J. Phys. Ref. Data Monograph No. 7*  
Zsargó, J., Federman, S. R. 1998, *ApJ*, 489, 256

TABLE 1  
ATMOSPHERIC AND OTHER OBSERVATIONAL PARAMETERS OF DI 1388

Star	$\alpha$ (J2000)	$\delta$ (J2000)	$V$	$B - V$	$T_{\text{eff}}$ kK	$\log g$ dex	$v_t$ $\text{km s}^{-1}$	$v_{\text{LSR}}^*$ $\text{km s}^{-1}$	$v \sin i$ $\text{km s}^{-1}$
DI 1388	02:57:12.94	-72:52:54.6	14.39	-0.26	$32 \pm 1$	$4.0 \pm 0.2$	$5 \pm 5$	$150 \pm 30$	$180 \pm 30$

Note. — Results are from Hambley et al. (1994) and references therein.

TABLE 2

LIST OF OBSERVED INTERSTELLAR ABSORPTION LINES IN THE DI 1388 SPECTRUM AND THEIR TOTAL EQUIVALENT WIDTHS AND COLUMN DENSITIES

Ions	$\lambda_{\text{lab}}^{\text{a}}$ Å	$f^{\text{a}}$	S/N	$W_{\text{MB}}$ mÅ	$\log N_{\text{MB}}$ cm $^{-2}$	Note
C I	1277.245	$9.67 \times 10^{-2}$	27	< 6.0	< 12.63	
	1328.833	$6.30 \times 10^{-2}$ <sup>b</sup>	33	< 5.2	< 12.72	
	1560.309	$8.04 \times 10^{-2}$	22	< 9.4	< 12.74	
	1656.928	$1.40 \times 10^{-1}$	14	< 15.4	< 12.65	
C II	1334.532	$1.28 \times 10^{-1}$	36	$232.7 \pm 10.5$	$> 14.87$	1
C II*	1335.708	$1.15 \times 10^{-1}$	38	$9.9 \pm 2.3$	$12.65 \pm 0.06$	
C IV	1550.770	$9.52 \times 10^{-2}$	22	$23.3 \pm 5.9$	$12.90 \pm 0.28$	2
N I	1199.550	$1.33 \times 10^{-1}$	17	$53.1 \pm 3.9$	$> 14.03$	
	1200.223	$8.85 \times 10^{-2}$	29	$42.0 \pm 3.3$	$> 13.82$	
	1200.710	$4.42 \times 10^{-2}$	21	$40.2 \pm 3.5$	$> 14.01$	
O I	1302.168	$4.89 \times 10^{-2}$	43	$168.9 \pm 10.1$	$> 14.83$	1
Mg II	1239.925	$6.17 \times 10^{-4}$ <sup>c</sup>	19	< 8.4	< 15.00	
	1240.395	$3.54 \times 10^{-4}$ <sup>c</sup>	19	< 8.4	< 15.24	
Al II	1670.787	1.83	14	190 :	$> 12.82$	3
Si II	1190.416	$2.50 \times 10^{-1}$	14	$140.1 \pm 11.8$	$> 14.07$	
	1193.290	$4.99 \times 10^{-1}$	20	$170.8 \pm 12.3$	$> 13.90$	
	1260.422	1.01	24	$220.4 \pm 18.6$	$14.23 :$	1
	1304.370	$8.60 \times 10^{-2}$ <sup>d</sup>	33	$113.2 \pm 11.8$	$14.20 \pm 0.08$	
	1526.706	$1.10 \times 10^{-1}$ <sup>d</sup>	24	$155.8 \pm 14.0$	$14.17 \pm 0.11$	
Si III	1206.500	1.67	28	$217.3 \pm 13.8$	$> 13.45$	1,2
Si IV	1393.755	$5.14 \times 10^{-1}$	32	$59.0 \pm 5.6$	$12.86 \pm 0.08$	2
	1402.770	$2.55 \times 10^{-1}$	27	$35.9 \pm 6.1$	$12.95 \pm 0.07$	2
P II	1152.818	$2.36 \times 10^{-1}$	5	< 31.2	< 13.05	
S II	1250.584	$5.45 \times 10^{-3}$	29	$13.1 \pm 1.4$	$14.20 \pm 0.14$	
	1253.811	$1.09 \times 10^{-2}$	27	$25 \pm 3.1$	$14.28 \pm 0.13$	
	1259.519	$1.62 \times 10^{-2}$	24	...	...	1
S III	1190.208	$2.22 \times 10^{-2}$	14	< 10.8	< 13.59	
Ca II	3934.777	$6.35 \times 10^{-1}$	39	$50.3 \pm 2.0$	$11.75 \pm 0.09$	
Mn II	1197.184	$1.57 \times 10^{-1}$	20	< 11.8	< 12.78	
Fe II	1260.533	$2.50 \times 10^{-2}$	33	36 :	$14.09 :$	1
	1608.451	$5.80 \times 10^{-2}$ <sup>e</sup>	20	$83.0 \pm 9.0$	$13.91 \pm 0.03$	
	1611.200	$1.02 \times 10^{-3}$ <sup>f</sup>	19	< 11.0	< 14.67	
Ni II	1317.217	$7.80 \times 10^{-2}$ <sup>g</sup>	30	< 5.8	< 12.68	
	1370.132	$7.70 \times 10^{-2}$ <sup>g</sup>	39	$5.2 \pm 4.7$	$12.66 \pm 0.20$	4
	1454.842	$2.98 \times 10^{-2}$ <sup>g</sup>	31	$5.5 \pm 5.2$	$12.57 \pm 0.40$	4

Note. — Uncertainties are  $1\sigma$  error (see text). Upper limits indicate that no feature is present and are  $3\sigma$  estimates (see text for more details). Lower limits indicate that the absorption line is saturated. A colon indicates that the value is uncertain. (1) Line blended with another interstellar absorption line or another velocity component. (2) Line is blended with the stellar line. (3) The MB component is only observed partly ( $\sim 70 - 80\%$ ). (4) Line very weak.

<sup>a</sup>Rest frame vacuum wavelengths and oscillator strengths are from Morton (1991), unless otherwise stated.

<sup>b</sup>From Wiese et al. (1996).

<sup>c</sup>From Sofia et al. (2000).

<sup>d</sup>From Spitzer and Fitzpatrick (1993); Dufton et al. (1983, 1992).

<sup>e</sup>From Mullman et al. (1997).

<sup>f</sup>From Cardelli and Savage (1995).

<sup>g</sup>From Fedchak and Lawler (1999); Zsargó and Federman (1998).

TABLE 3  
COMPONENT FITTING MEASUREMENTS AT  $\sim 179$  AND  $\sim 198$   $\text{km s}^{-1}$

Ions	$\lambda_{\text{lab}}$ (Å)	$b$ ( $\text{km s}^{-1}$ )		$\log N$ ( $\text{cm}^{-2}$ )	
		179 $\text{km s}^{-1}$	198 $\text{km s}^{-1}$	179 $\text{km s}^{-1}$	198 $\text{km s}^{-1}$
C II	1334.532	12.0 :	8.0 :	> 14.54	> 14.60
N I	1200.223	...	$4.5 \pm 0.6$	...	$14.00 \pm 0.12$
	1200.710	11 :	$5.1 \pm 0.5$	$13.05 \pm 0.19$	> 14.07
O I	1302.168	$10.7 \pm 0.3$	$6.7 \pm 0.3$	> 14.44	> 14.51
Al II	1670.787	11.7 :	8.7 :	> 12.5 :	> 12.6 :
Si II	1304.370	$10.9 \pm 0.4$	$7.6 \pm 0.4$	$13.68 \pm 0.06$	$14.06 \pm 0.03$
	1526.706	$10.6 \pm 0.4$	$6.6 \pm 0.4$	$13.73 \pm 0.07$	$14.00 \pm 0.05$
S II	1250.584	$7.1 \pm 1.2$	$5.1 \pm 1.2$	$13.67 \pm 0.15$	$14.11 \pm 0.08$
Ca II	3933.663	$12.7 \pm 0.7$	$7.8 \pm 0.6$	$10.93 \pm 0.17$	$11.73 \pm 0.05$
Fe II	1608.451	$10.0 \pm 0.5$	$6.0 \pm 0.5$	$13.38 \pm 0.05$	$13.77 \pm 0.04$

TABLE 4  
SUMMARY OF DEPLETIONS OF THE MB TOWARD DI 1388

Ions	MB			Galactic Depletions			SMC	LMC
	$X^i$	$\log \left(\frac{X}{S}\right)_c^a$	$\log(N(X^i))^b$	$D(X)$	Cold <sup>c</sup>	Warm <sup>c</sup>	Halo <sup>d</sup>	
C II	+1.28	> 14.87	> -0.65	-0.4	-0.4	(-0.4)	-0.14	+0.06
N I	+0.70	> 14.00	> -0.94	-0.1	-0.1	(-0.1)	-0.66	-0.26
O I	+1.60	> 14.83	> -1.01	-0.4	-0.4	(-0.4)	-0.16	+0.05
Mg II	+0.31	< 15.00	< +0.45	-1.2	-0.6	-0.3	+0.08	+0.44
Al II	-0.79	> 12.82	> -0.63	-2.4	-1.1	(-0.6)	+0.20	+0.19
Si II	+0.28	$14.19 \pm 0.14$	$-0.33 \pm 0.16$	-1.3	-0.4	-0.3	+0.16	+0.02
P II	-1.70	< 13.05	< +0.51	-0.5	-0.2	(-0.1)	...	...
Mn II	-1.74	< 12.78	< +0.28	-1.5	-1.0	-0.7	+0.18	+0.25
Fe II	+0.24	$13.91 \pm 0.05$	$-0.57 \pm 0.19$	-2.2	-1.4	-0.6	+0.01	+0.29
Ni II	-1.02	$12.52 \pm 0.20$	$-0.70 \pm 0.25$	-2.2	-1.4	-0.6	+0.28	+0.36

Note. — (a) Solar system meteoritic abundances from Anders and Grevesse (1989) except for C, N and O, which are photospheric values from Grevesse and Noels (1993);  $\log(S/H)_c = -4.73$ . (b) Adopted S II column density,  $\log(N(S^+)) = 14.24 \pm 0.19$  dex. (c) Updated from Jenkins (1987), see Lauroesch et al. (1996); Welty et al. (1997, 1999b). (d) From Savage and Sembach (1996); Fitzpatrick (1996); and references therein. Values in parentheses are estimated, see Welty et al. (1997, 1999b). For Ni II, the depletions were corrected to take into account the new oscillator strength scaling. (e)  $[X/S] = \log(X/S)_{\text{SMC/LMC}} - \log(X/S)_c$  (Russell and Dopita (1992) but adjusted for C, N and O photospheric values, and Al abundances are from Welty et al. (1997, 1999a), while LMC Si abundance is from Korn and Wolf (1999), but see also discussion in Garnett (1999)).

TABLE 5  
OBSERVED DEPLETIONS FOR THE TWO MB CLOUDS AT 179 AND 198  $\text{km s}^{-1}$ .

Ions	$X^i$	MB Depletions		Galactic Depletions <sup>a</sup>		
		$\log \left(\frac{X}{S}\right)_c$	$D_{179}(X)$	$D_{198}(X)$	Cold	Warm
C II	+1.28	$> -0.41$	$> -0.79$	-0.4	-0.4	(-0.4)
N I	+0.70	$-1.32 \pm 0.23$	$> -0.79$	-0.1	-0.1	(-0.1)
O I	+1.60	$> -0.83$	$> -1.20$	-0.4	-0.4	(-0.4)
Al II	-0.79	$> -0.43 :$	$> -0.74 :$	-2.4	-1.1	(-0.6)
Si II	+0.28	$-0.25 \pm 0.16$	$-0.36 \pm 0.09$	-1.3	-0.4	-0.3
Fe II	+0.24	$-0.53 \pm 0.16$	$-0.58 \pm 0.09$	-2.2	-1.4	-0.6

Note. — (a) Values in parentheses are estimated. See footnote in Table 4 and text for references.

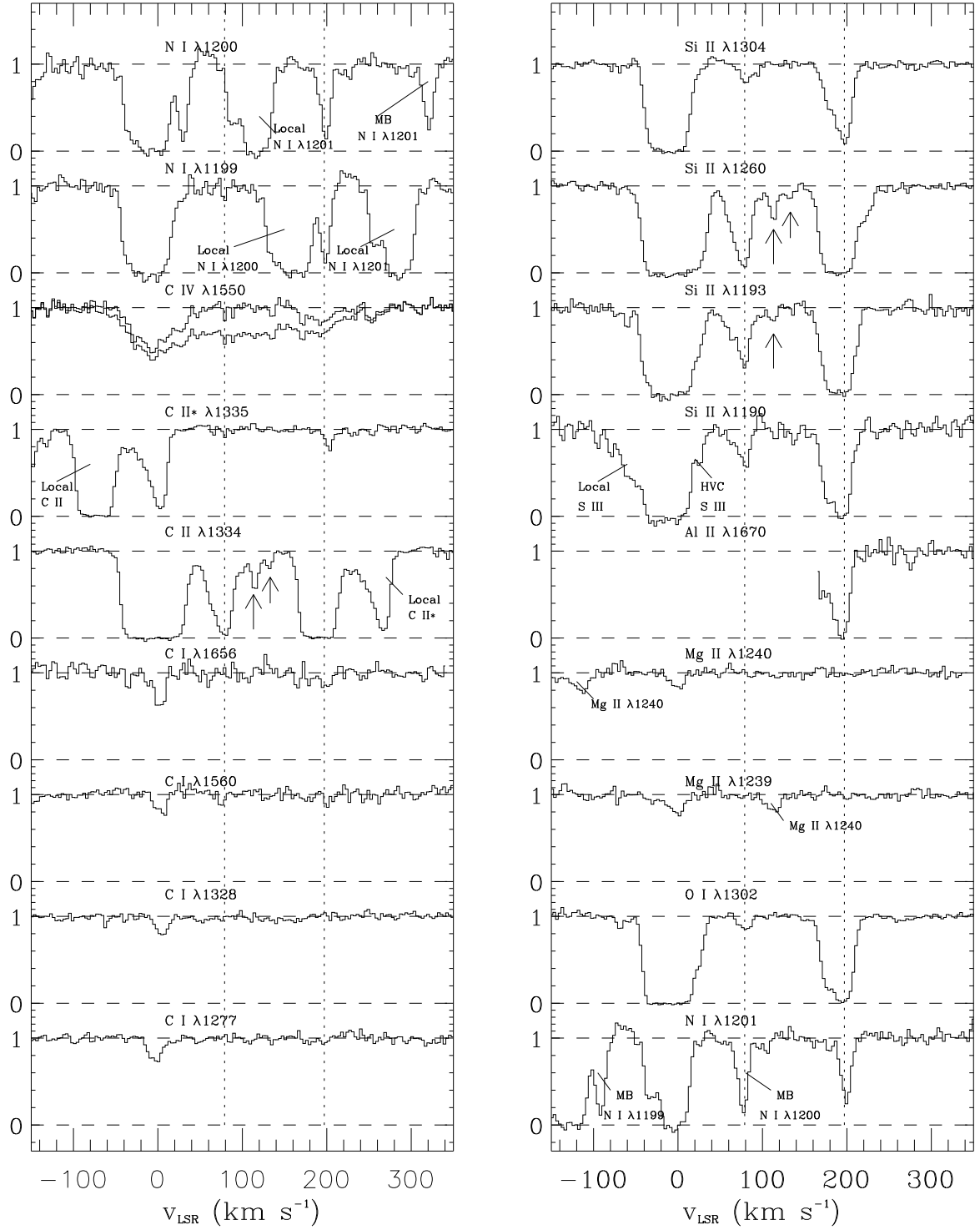


FIG. 1.— Normalized profiles of absorption lines in the *HST* STIS spectrum of DI 1388 plotted against LSR velocity. Absorption from the Magellanic Bridge is detected at  $\sim 200 \text{ km s}^{-1}$ , while the HVC discussed by Lehner et al. (2000) is at  $\sim 80 \text{ km s}^{-1}$ . The arrows indicate the detection of two other weak HVCs at 113 and 130  $\text{km s}^{-1}$ . For C IV and Si IV, we have indicated the observed line profile (lower profile) and the interstellar feature deblended from the stellar line spectrum (see text for more detailed information).

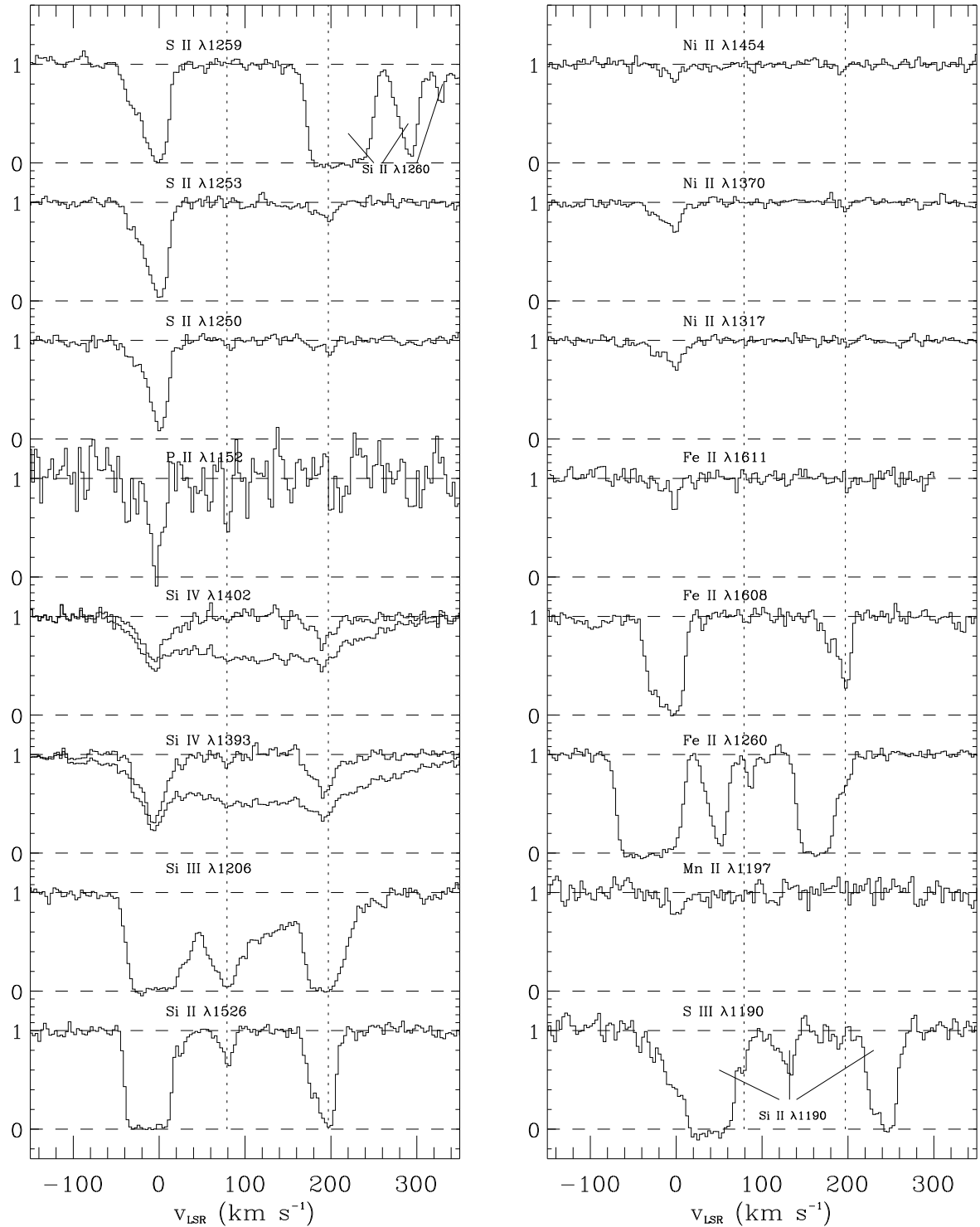


FIG. 1.— continued.

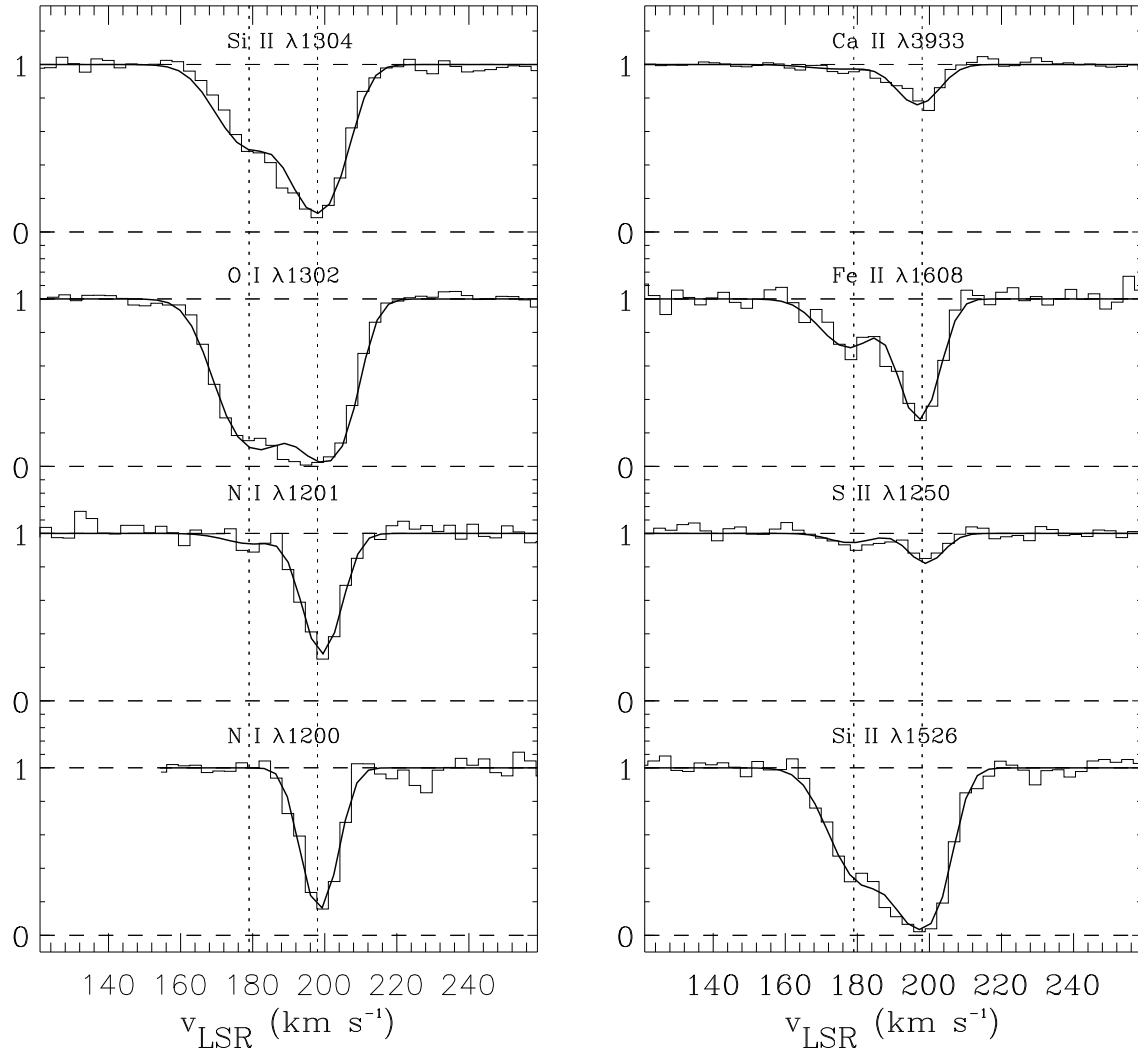


FIG. 2.— Histograms are the observed spectra. Smooth lines are the fits with two Voigt components (except for N I  $\lambda 1200$  where one component is sufficient). Dotted lines show the component centroids at  $179$  and  $198$   $\text{km s}^{-1}$ . The fit for O I is relatively poor in comparison with the others, indicating that the sharp component has some unresolved saturated structures or perhaps additional weak components.

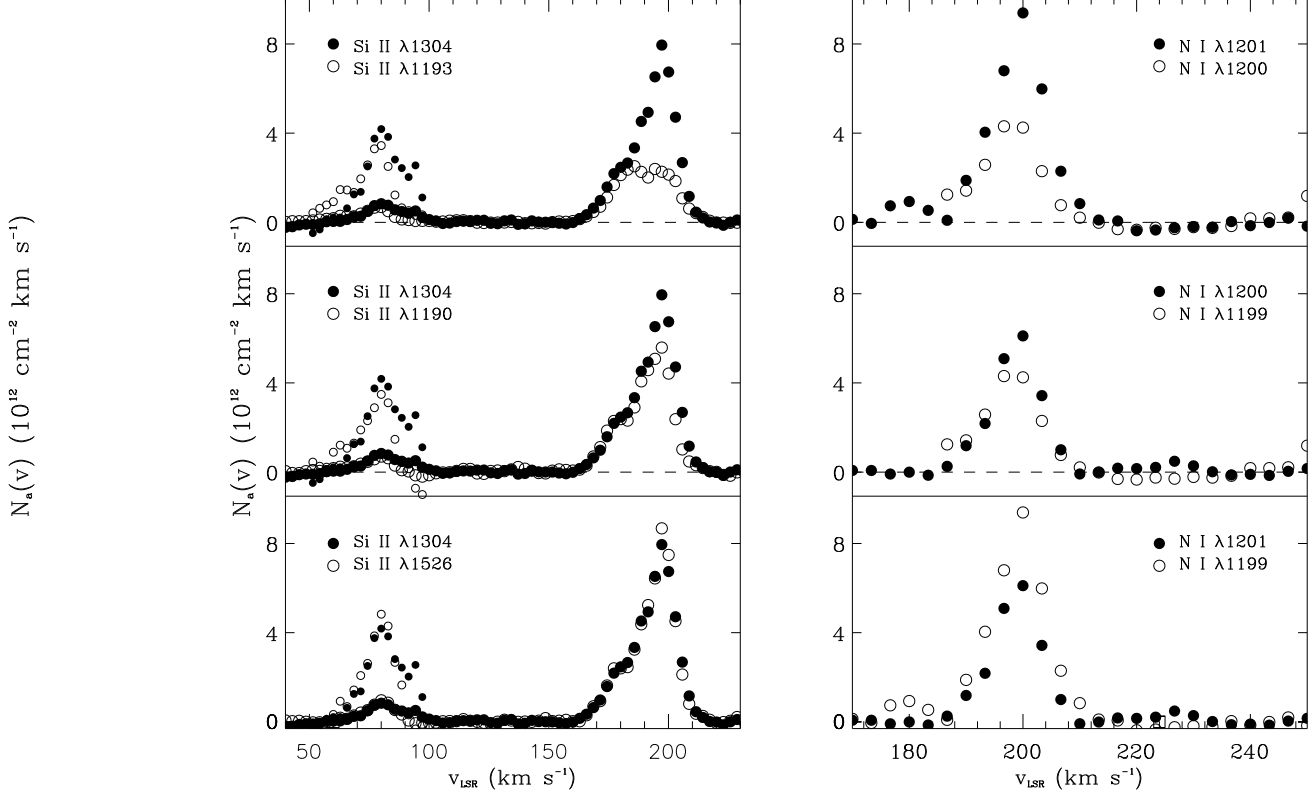


FIG. 3.— Profiles of apparent column density of Si II and N I versus  $v_{\text{LSR}}$  at the HVC ( $80 \text{ km s}^{-1}$ ) and MB ( $200 \text{ km s}^{-1}$ ) absorption toward DI 1388. The smaller circles at the velocities of the HVC absorption show the same profiles expanded by a factor of 5 in the vertical scale. The MB N I  $\lambda 1199$  is blended with the local N I  $\lambda 1200$ : therefore for  $\lambda 1199$  transition, we only plot the apparent column density when  $v_{\text{LSR}} > 180 \text{ km s}^{-1}$ .

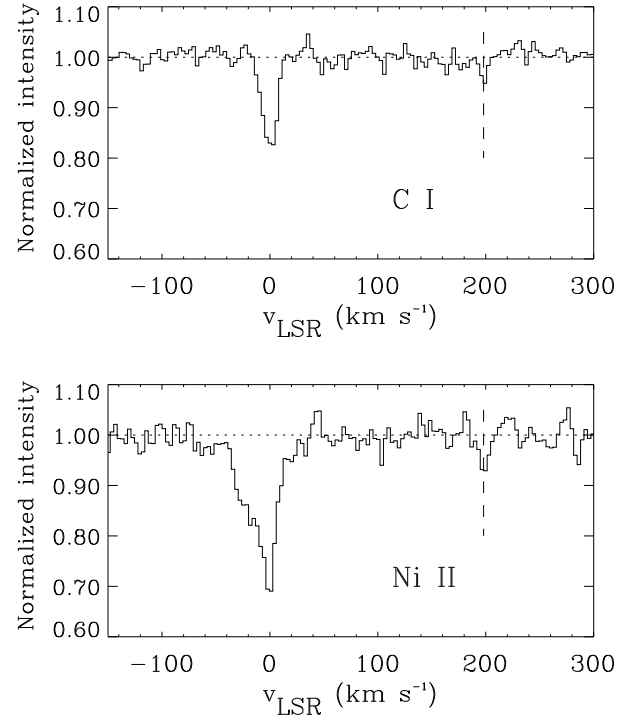


FIG. 4.— Histograms of the co-added spectra for C I and Ni II.

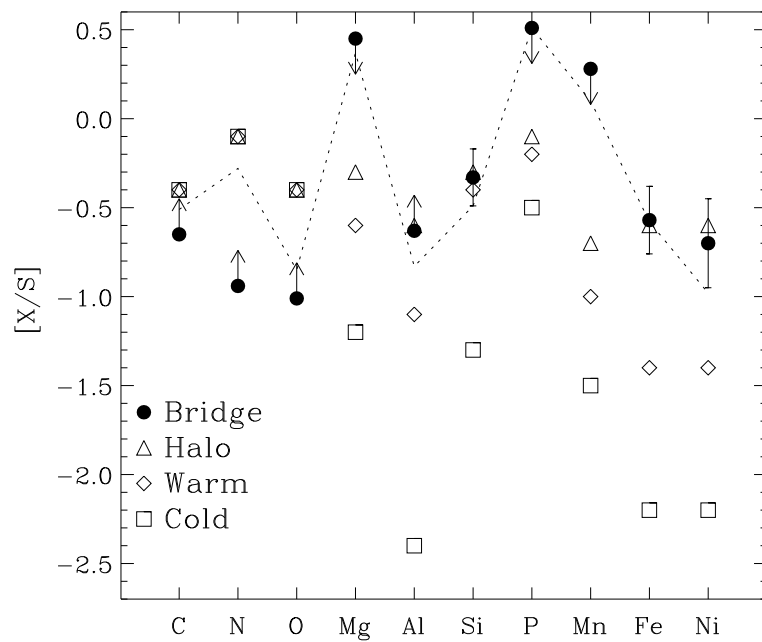


FIG. 5.— Relative gas-phase abundances for the MB (DI 1388 sight line), with respect to sulfur, compared to relative abundances found in Galactic cold, warm and halo clouds. Error bars are  $1\sigma$ . The upward (downward) arrows indicate lower (upper) limits. The Dotted line represents the MB depletions corrected from the underlying (undepleted) total elemental relative abundance patterns of the SMC with respect to the Galaxy.

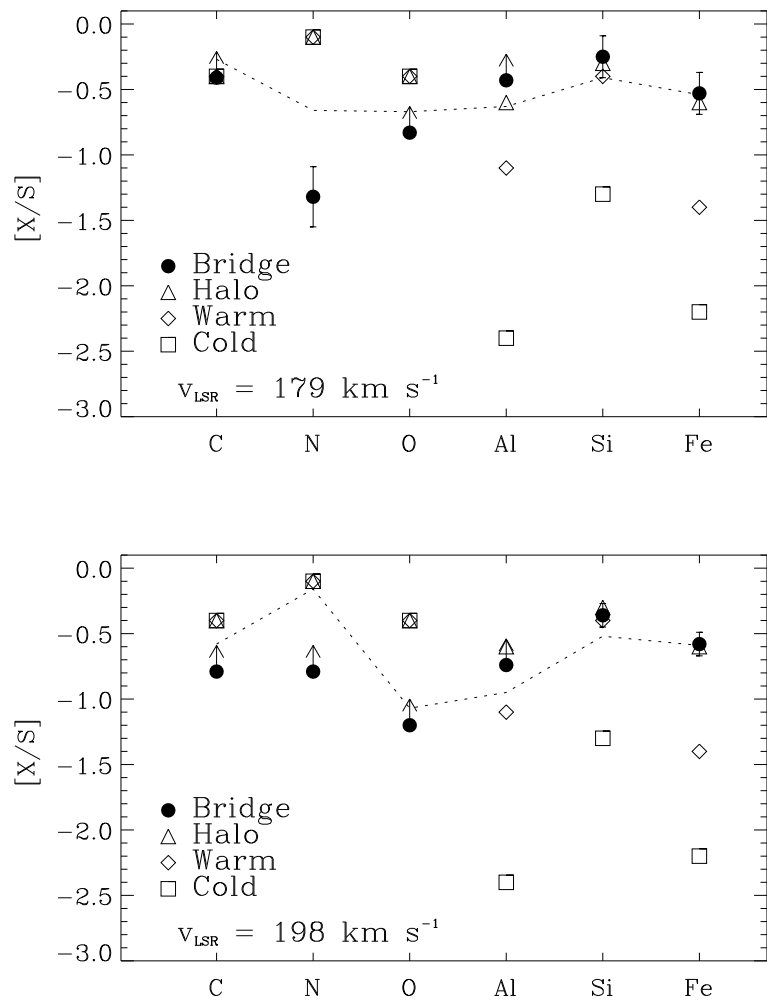


FIG. 6.— Same as Figure 5, but for the two clouds at  $179$  and  $198 \text{ km s}^{-1}$ .

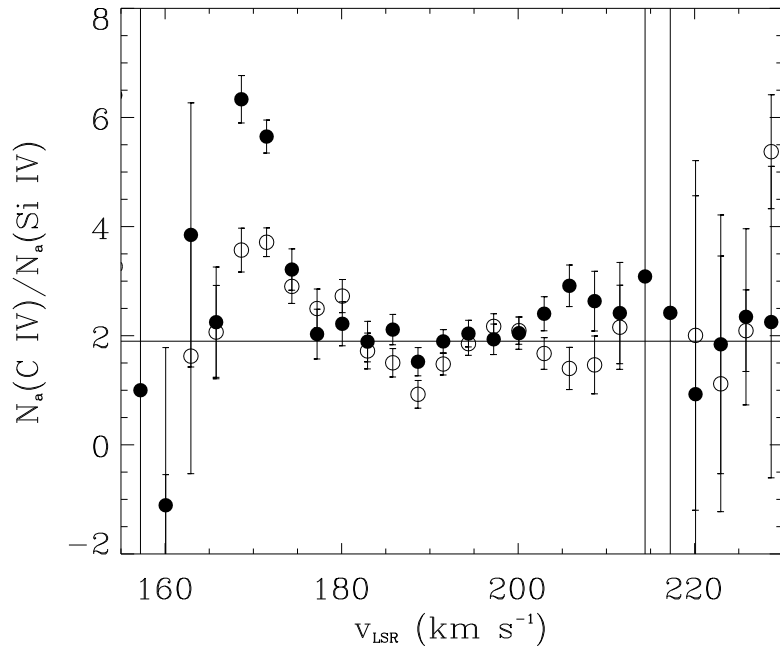


FIG. 7.—  $N_a(\text{C}^{+3})/N_a(\text{Si}^{+3})$  line ratio versus LSR velocity in the MB component. Open circles correspond to the comparison of C IV  $\lambda 1550$  with Si IV  $\lambda 1393$ , and filled circles correspond to the comparison of C IV  $\lambda 1550$  with Si IV  $\lambda 1402$ . The solid line is the mean value of this ratio in the velocity range of  $180$  and  $200$   $\text{km s}^{-1}$ .